Proceedings of Machine Learning Research tbd:1–29, 2025 International Conference on Computational Optimization

The Ky Fan Norms and Beyond: Dual Norms and Combinations for Matrix Optimization

Alexey Kravatskiy KRAVTSKII.AIU@PHYSTECH.EDU
MIPT

Ivan Kozyrev KOZYREV.IN@PHYSTECH.EDU
MIPT, INM RAS

Nikolai Kozlov KOZLOV.NA@PHYSTECH.EDU
MIPT

Alexander Vinogradov VINOGRADOV.AM@PHYSTECH.EDU
MIPT

Daniil Merkulov DANIIL.MERKULOV@PHYSTECH.EDU
MIPT, Skoltech, HSE, AI4Science

Ivan Oseledets I.OSELEDETS@SKOLTECH.RU
AIRI, Skoltech, INM RAS

Abstract

In this article, we explore the use of various matrix norms for optimizing functions of weight matrices, a crucial problem in training large language models. Moving beyond the spectral norm underlying the Muon update, we leverage duals of the Ky Fan k-norms to introduce a family of Muon-like algorithms we name *Fanions*, which are closely related to Dion. By working with duals of convex combinations of the Ky Fan k-norms with either the Frobenius norm or the l_∞ norm, we construct the families of *F-Fanions* and *S-Fanions*, respectively. Their most prominent members are *F-Muon* and *S-Muon*. We complement our theoretical analysis with an extensive empirical study of these algorithms across a wide range of tasks and settings, demonstrating that F-Muon and S-Muon consistently match Muon's performance, while outperforming vanilla Muon on synthetic linear least squares problems.

1. Introduction

Minimizing loss functions in unprecedentedly high-dimensional spaces has recently become an integral and crucial part in training large language models. Hence, new scalable, time- and memory-efficient algorithms have been demanded. Besides well-known Adam (Kingma and Ba, 2014) and AdamW (Loshchilov and Hutter, 2017), recently proposed Muon (Jordan et al., 2024b) has shown promising results on training very large models (Liu et al., 2025). Its key difference from Adam and AdamW is that it has been constructed specifically for optimizing functions of weight matrices, which are common in deep learning.

From a theoretical perspective, a key innovation of Muon was its principled derivation of the update rule, which emerged as the solution to an optimization problem constrained by the RMS-to-RMS norm (a scaled version of the spectral norm) (Bernstein, 2025).

Motivated by the success of Muon, many generalizations and variations of it were proposed. Among the notable ones are Scion (Pethick et al., 2025c), Dion (Ahn et al., 2025) and Gluon (Riabinin et al., 2025). Those works try to explain Muon's efficiency and establish convergence bounds. One central question, however, remains unanswered:

In deriving Muon's update step, why should one constrain by the spectral or any other operator norm? How would alternative norms affect performance and computational cost?

In this article, we tackle this question by showing that there are many viable non-operator norms. We leverage the family of norms dual to Ky Fan k-norms to derive a new family of *Fanions*, algorithms with low-rank updates. This approach theoretically explains the backbone of Dion's update (Ahn et al., 2025) and generalizes the memory-motivated application of the nuclear norm to Sharpness-Aware Minimization (Pethick et al., 2025b). As was done with Muon, we develop an effective procedure for computing Fanions' updates. The Lanczos algorithm, which is described and compared with its competitors in Section 5, is the most operation-efficient algorithm, though it currently lacks an effective GPU- and PyTorch-friendly implementation.

Working with dual norms and various convex combinations of norms, we construct the families of *F-Fanions* and *S-Fanions*, which are hybrids of Muon with NormalizedSGD and SignSGD, respectively.

We then compare the performance of these algorithm families on various model and real-world problems:

- Synthetic least squares experiment Section 6.1
- CIFAR-10 airbench (Keller, 2023)
- Pre-training NanoGPT on FineWeb dataset (Jordan et al., 2024a)
- Fine-tuning NanoGPT on Tiny Stories (Eldan and Li, 2023)

Our experiments reveal important insights into the role of matrix norms in optimization. First, using the example of Neon (the rank-one Fanion), we show that not every LMO-based algorithm is effective, despite sharing the same asymptotics in the general bounds of (Kovalev, 2025) and (Riabinin et al., 2025). This suggests that existing theoretical guarantees should be refined to better explain empirical performance.

Most notably, our experiments on real-world tasks demonstrate that the choice of underlying matrix norm is remarkably flexible. On CIFAR-10 airbench, properly-tuned F-Muon and S-Muon achieve $94.02 \pm 0.13\%$ and $94.03 \pm 0.13\%$ accuracy, matching Muon's $94.01 \pm 0.13\%$ performance. On NanoGPT pre-training, F-Muon achieves 3.281 cross-entropy loss, while fully-tuned Muon achieves 3.279. Finally, S-Muon matches Muon on fine-tuning NanoGPT on Tiny Stories, while F-Muon is far more resistant to learning rate choice than Muon. These results show that Muon-like algorithms can maintain competitive performance even when the underlying norm constraint is significantly modified, providing an affirmative answer to the central question posed above. Moreover, the tools from Section 4 give researchers considerable flexibility in designing algorithms that need not be direct modifications of Muon.

2. Preliminaries: Linear Minimization Oracle Framework

Training a neural network is essentially an optimization of a function of several weight matrices and a few vectors. Let us start by considering the problem of minimizing a differentiable function of a *single* matrix:

$$F(\cdot)\colon \mathbb{R}^{m\times n} \to \mathbb{R}\,, \qquad F(\boldsymbol{X}) \to \min_{\boldsymbol{X}\in\mathbb{R}^{m\times n}} \tag{1}$$

We equip the matrix space $\mathbb{R}^{m\times n}$ with a standard dot product $\langle\cdot,\cdot\rangle \to \mathbb{R}$ and a norm $\|\cdot\|\colon \mathbb{R}^{m\times n} \to \mathbb{R}_+$, which does not have to coincide with the Frobenius norm $\|\cdot\|_{\mathrm{F}} = \langle\cdot,\cdot\rangle$. The dual norm $\|\cdot\|^\dagger\colon \mathbb{R}^{m\times n} \to \mathbb{R}_+$ that is associated with $\|\cdot\|$ is defined as

$$\|\boldsymbol{G}\|^\dagger = \sup_{\boldsymbol{D}\in\mathbb{R}^{m\times n}\,:\|\boldsymbol{D}\|\le 1} \langle \boldsymbol{G}, \boldsymbol{D}\rangle\,. \tag{2}$$

Such problems can be solved with an iterative algorithm based on the Linear Minimization Oracle (LMO):

$$\mathrm{LMO}(\boldsymbol{M}^t) \in \arg\min_{\boldsymbol{D}\in\mathcal{S}} \langle \boldsymbol{M}^t, \boldsymbol{D}\rangle\,, \tag{3}$$

where $\boldsymbol{M}^t$ is the gradient (or momentum) of F at $\boldsymbol{X}^t$ and $\mathcal{S} \subset \mathbb{R}^{m\times n}$ is some set. The update of the algorithm is defined as follows:

$$\boldsymbol{X}^{t+1} = \boldsymbol{X}^t + \gamma_t \mathrm{LMO}\left(\boldsymbol{M}^t\right)\,. \tag{4}$$

We are particularly interested in the case when $\mathcal{S}$ is a unit ball in some norm $\|\cdot\|$:

$$\mathcal{S} = \mathcal{B}_{\|\cdot\|} = \{\boldsymbol{D} \in \mathbb{R}^{m\times n} \mid \|\boldsymbol{D}\| \le 1\}\,.$$

In this case,

$$\arg\min_{\boldsymbol{D}\in\mathcal{S}} \langle \boldsymbol{M}^t, \boldsymbol{D}\rangle = -\{\boldsymbol{D} \in \mathcal{B}_{\|\cdot\|} \mid \langle \boldsymbol{M}^t, \boldsymbol{D}\rangle = \|\boldsymbol{M}^t\|^\dagger\}\,,$$

and the update for $\boldsymbol{X}^t$ in Equation (4) simplifies to

$$\boldsymbol{X}^{t+1} = \boldsymbol{X}^t - \gamma_t\{\boldsymbol{D} \in \mathcal{B}_{\|\cdot\|} \mid \langle \boldsymbol{M}^t, \boldsymbol{D}\rangle = \|\boldsymbol{M}^t\|^\dagger\}\,. \tag{5}$$

Using this formula, it is easy to compute updates for algorithms induced by various norms $\|\cdot\|$:

Frobenius norm and Normalized SGD When the norm $\|\cdot\|$ is the Frobenius norm $\|\cdot\|_{\mathrm{F}}$, Equation (5) turns into

$$\boldsymbol{X}^{t+1} = \boldsymbol{X}^t - \gamma_t \frac{\boldsymbol{M}^t}{\|\boldsymbol{M}^t\|_{\mathrm{F}}}\,, \tag{6}$$

which recovers Normalized SGD (NSGD).

Spectral norm and Muon When the norm is the spectral norm $\|\cdot\|_2$, we get

$$\boldsymbol{X}^{t+1} = \boldsymbol{X}^t - \gamma_t \boldsymbol{U}\boldsymbol{V}^\top\,, \tag{7}$$

which is Muon without the $\sqrt{m/n}$ factor. Here, $\boldsymbol{M}^t = \boldsymbol{U}\boldsymbol{\Sigma}\boldsymbol{V}^\top$ is the Singular Value Decomposition (SVD) of $\boldsymbol{M}^t$ ($\boldsymbol{U} = [\boldsymbol{u}_1, \boldsymbol{u}_2, \ldots, \boldsymbol{u}_r]$, $\boldsymbol{\Sigma} = \mathrm{diag}(\sigma_1, \sigma_2, \ldots, \sigma_r)$, and $\boldsymbol{V} = [\boldsymbol{v}_1, \boldsymbol{v}_2, \ldots, \boldsymbol{v}_r]$). Muon can be recovered by taking the RMS-to-RMS norm: $\sqrt{n/m}\|\cdot\|_2$.

Chebyshev norm and SignSGD When the norm is the Chebyshev norm $\|\cdot\|_{\mathrm{C}}$, we get

$$\boldsymbol{X}^{t+1} = \boldsymbol{X}^t - \gamma_t \operatorname{sign}(\boldsymbol{M}^t)\,, \tag{8}$$

which recovers SignSGD (Bernstein et al., 2018). Here, $\operatorname{sign}(\boldsymbol{M}^t)$ denotes the element-wise sign function. SignSGD is particularly notable for its communication efficiency in distributed training, as it compresses gradients to 1-bit per parameter.

3. Beyond the Spectral Norm: Fanions

3.1. The Rank Gap Problem

Having examined the Frobenius norm (NSGD), spectral norm (Muon), and Chebyshev norm (SignSGD), all of which produce full-rank updates, we turn to the nuclear norm $\|\cdot\|_*$.

Lemma 1 *When $\|\cdot\| = \|\cdot\|_*$, Equation (5) becomes*

$$\boldsymbol{X}^{t+1} = \boldsymbol{X}^t - \gamma_t \boldsymbol{u}_1 \boldsymbol{v}_1^\top\,. \tag{9}$$

Proof Since $\|\cdot\|_*^\dagger = \|\cdot\|_2$, the goal is to reach $\langle \boldsymbol{M}^t, \boldsymbol{D}\rangle = \sigma_1$ in Equation (5). Note that $\boldsymbol{D} = \boldsymbol{u}_1 \boldsymbol{v}_1^\top$ delivers this value. Indeed, $\|\boldsymbol{D}\|_* = 1$ and by the trace property and orthogonality of the singular vectors,

$$\langle \boldsymbol{M}^t, \boldsymbol{D}\rangle = \langle \boldsymbol{U}\boldsymbol{\Sigma}\boldsymbol{V}^\top, \boldsymbol{u}_1\boldsymbol{v}_1^\top\rangle = \operatorname{tr}\operatorname{diag}(\sigma_1, 0, \ldots, 0) = \|\boldsymbol{M}^t\|_2\,,$$

which completes the proof. ■

We call this algorithm *Neon*. The nuclear norm thus yields rank-one updates, in stark contrast to the full-rank updates of Muon, NSGD, and SignSGD. This raises a natural question: can we derive algorithms with updates of intermediate ranks?

Schatten norms (Cesista, 2025) considered Schatten-p norms:

$$\|\boldsymbol{M}^t\|_{S_p} = \left(\sum_{i=1}^{\min(m,n)} \sigma_i^p\right)^{1/p}\,,$$

which produce the update

$$\boldsymbol{X}^{t+1} = \boldsymbol{X}^t - \gamma_t \boldsymbol{U} \frac{\operatorname{diag}\left(\sigma_1^{q-1}, \ldots, \sigma_{\min(m,n)}^{q-1}\right)}{\left(\sum_{i=1}^{\min(m,n)} \sigma_i^q\right)^{\frac{q-1}{q}}} \boldsymbol{V}^\top$$

where p and q satisfy $p^{-1} + q^{-1} = 1$. This formula recovers Neon when $p \to 1$ (provided $\sigma_1 > \sigma_2$, which holds on real data), NSGD when $p = 2$, and Muon when $p \to \infty$.

However, Schatten norms do not fill the rank gap: when $p > 1$, the update has full rank, while when $p = 1$, it has rank one. Moreover, computing the update for $p \neq 1, 2, \infty$ appears to require knowing all σ_i, making the problem as hard as computing the full SVD.

Ky Fan norms Another family of matrix norms offers a potential solution: the Ky Fan norms. For $k \in \{1, \dots, \min(m,n)\}$, the Ky Fan k-norm $\|\cdot\|_{\text{KF-}k}$ equals $\sum_{i=1}^{k} \sigma_i$, the sum of the k largest singular values. Notable special cases include the Ky Fan 1-norm (the spectral norm) and the Ky Fan $\min\{m,n\}$-norm (the nuclear norm).

To derive the update formula for arbitrary k, we use the expression for the norm dual to the Ky Fan k-norm (see, for instance (Bhatia, 2013), p. 96):

$$\|\cdot\|_{\text{KF-}k}^{\dagger} = \max\left\{\frac{1}{k}\|\cdot\|_*, \|\cdot\|_2\right\}.$$

According to Equation (5), we need to find $\boldsymbol{D}$ such that $\|\boldsymbol{D}\|_{\text{KF-}k} = 1$ and

$$\langle \boldsymbol{M}^t, \boldsymbol{D}\rangle = \max\left\{\frac{1}{k}\sum_{i=1}^{\min(m,n)} \sigma_i,\ \sigma_1\right\}.$$

The Neon update $\boldsymbol{D} = \boldsymbol{u}_1\boldsymbol{v}_1^\top$ achieves σ_1, while the scaled Muon update $\boldsymbol{D} = \frac{1}{k}\sum_{i=1}^{\min(m,n)} \boldsymbol{u}_i\boldsymbol{v}_i^\top$ achieves $\frac{1}{k}\sum_{i=1}^{\min(m,n)} \sigma_i$. Thus, the update is either

$$\boldsymbol{X}^{t+1} = \boldsymbol{X}^t - \gamma_t \boldsymbol{u}_1\boldsymbol{v}_1^\top \text{ or } \boldsymbol{X}^{t+1} = \boldsymbol{X}^t - \frac{\gamma_t}{k}\boldsymbol{U}\boldsymbol{V}^\top,$$

depending on which of those two expressions achieves smaller residual on the linear function $L(\boldsymbol{X}) := F(\boldsymbol{X}^t) + \langle \boldsymbol{M}^t, \boldsymbol{X} - \boldsymbol{X}^t\rangle$. The Ky Fan norms thus fail to close the rank gap: the resulting update is either rank-one or full-rank.

3.2. Solution: Duals to Ky Fan Norms

Unlike Schatten norms, which satisfy $\|\boldsymbol{M}^t\|_{S_p}^{\dagger} = \|\boldsymbol{M}^t\|_{S_q}$ (for $p^{-1} + q^{-1} = 1$) and are thus closed under dualization, Ky Fan norms are generally not. Only two exceptional cases exist: the dual of the Ky Fan 1-norm $\|\cdot\|_{\text{KF-}1}$ (the spectral norm) is the Ky Fan $\min(m,n)$-norm $\|\cdot\|_{\text{KF-}\min(m,n)}$ (the nuclear norm), and vice versa. Thus working with duals of Ky Fan norms can open up new possibilities:

Lemma 2 *When $\|\cdot\| = \|\boldsymbol{M}^t\|_{\text{KF-}k}^{\dagger}$, Equation (5) turns into:*

$$\boldsymbol{X}^{t+1} = \boldsymbol{X}^t - \gamma_t \sum_{i=1}^{k} \boldsymbol{u}_i\boldsymbol{v}_i^\top. \tag{10}$$

Proof Since $\|\cdot\|^{\dagger} = \|\cdot\|_{\text{KF-}k}^{\dagger\dagger} = \|\cdot\|_{\text{KF-}k}$, the goal is to reach $\langle \boldsymbol{M}^t, \boldsymbol{D}\rangle = \|\boldsymbol{M}^t\|_{\text{KF-}k}$ in Equation (5). Note that $\boldsymbol{D} = \sum_{i=1}^{k} \boldsymbol{u}_i\boldsymbol{v}_i^\top$ attains this value. Indeed,

$$\langle \boldsymbol{M}^t, \boldsymbol{D}\rangle = \langle \boldsymbol{U}\boldsymbol{\Sigma}\boldsymbol{V}^\top, \sum_{i=1}^{k} \boldsymbol{u}_i\boldsymbol{v}_i^\top\rangle = \sum_{i,j=1}^{r,k} \langle \boldsymbol{u}_i\sigma_i\boldsymbol{v}_i^\top, \boldsymbol{u}_j\boldsymbol{v}_j^\top\rangle = \sum_{i=1}^{k}\sigma_i = \|\boldsymbol{M}^t\|_{\text{KF-}k},$$

which completes the proof. ■

These updates define the *Fanion* family of LMO-based algorithms, each operating under a norm $\|\boldsymbol{M}^t\|_{\text{KF-}k}^{\dagger}$. We denote the algorithm for a particular k as *Fanion-k*. This family elegantly bridges the rank gap, providing updates of any intermediate rank k.

Connection to existing algorithms The Fanion family unifies several known algorithms:

- **Neon** is Fanion-1 (rank-one updates)
- **Muon** is Fanion-$\min\{m, n\}$ (full-rank updates)
- **Dion** (unsharded): The rank-r Dion (Algorithm 1 from (Ahn et al., 2025)) without error feedback and without scaling of the update is actually Fanion-r (see (Pethick, 2025), where Dion is written in a notation more similar to ours)

In Section 5, we will discuss how to efficiently compute Fanion updates using the Lanczos algorithm.

4. Conic Combination of LMO-algorithms is an LMO-algorithm

Simply applying norms dual to Ky Fan k-norms, however, does not provide sufficient algorithmic diversity for our purposes. We now consider linear combinations of LMO-based algorithms and show that these combinations are themselves LMO-algorithms.

4.1. General Case

We begin with a well-known result on dual norms (see, e.g., (Yu, 2012, Table 1)).

Lemma 3 *Let $\|\cdot\|_{(1)}, \dots, \|\cdot\|_{(n)}$ be norms on a finite-dimensional Euclidean space, and let $\alpha_1, \dots, \alpha_n$ be non-negative reals. Define*

$$\|\cdot\| := \sum_{i=1}^{n} \alpha_i \|\cdot\|_{(i)}.$$

Then the dual unit ball of $\|\cdot\|$ satisfies

$$\mathcal{B}_{\|\cdot\|^\dagger} = \sum_{i=1}^{n} \alpha_i \mathcal{B}_{\|\cdot\|^\dagger_{(i)}}$$

where $\sum$ denotes the Minkowski sum and $\mathcal{B}_{\|\cdot\|^\dagger_{(i)}}$ is the unit ball of the dual norm $\|\cdot\|^\dagger_{(i)}$.

A proof is provided in the appendix (see Section C).

Lemma 4 *Let $\|\cdot\|_{(1)}, \dots, \|\cdot\|_{(n)}$ be norms on a finite-dimensional Euclidean space, and let $\alpha_1, \dots, \alpha_n$ be non-negative reals. Consider Linear Minimization Oracles $\mathrm{LMO}_1, \dots, \mathrm{LMO}_n$, corresponding to the unit balls of these norms. Then, $\sum_{i=1}^n \alpha_i \mathrm{LMO}_i$ is the LMO corresponding to the norm $\|\cdot\|$ dual to the $\sum_{i=1}^n \alpha_i \|\cdot\|^\dagger_{(i)}$.*

Proof Using Lemma 3 and the biduality property $\|\cdot\|^{\dagger\dagger} = \|\cdot\|$, we obtain the unit ball representation: $\mathcal{B}_{\|\cdot\|} = \sum_{i=1}^n \alpha_i \mathcal{B}_{\|\cdot\|_{(i)}}$. The linear minimization problem over this ball can thus be transformed as follows:

$$\arg\min_{\boldsymbol{D} \in \mathcal{B}_{\|\cdot\|}} \langle \boldsymbol{M}, \boldsymbol{D} \rangle = \arg\min_{\boldsymbol{D}_1 \in \alpha_i \mathcal{B}_{\|\cdot\|_{(1)}}, \dots, \boldsymbol{D}_n \in \alpha_n \mathcal{B}_{\|\cdot\|_{(n)}}} \langle \boldsymbol{M}, \sum_{i=1}^{n} \boldsymbol{D}_i \rangle = \sum_{i=1}^{n} \arg\min_{D_i \in \mathcal{B}_{\|\cdot\|_{(i)}}} \langle \boldsymbol{M}, \boldsymbol{D}_i \rangle,$$

where the last summation denotes the Minkowski sum. This immediately implies $\sum_{i=1}^{n} \alpha_i \mathrm{LMO}_i \in \arg\min_{\boldsymbol{D}\in\mathcal{B}_{\|\cdot\|}} \langle \boldsymbol{M}, \boldsymbol{D}\rangle$, completing the proof. ■

Applying this result to optimization algorithms yields the following corollary.

Corollary 5 *Let there be a finite family of LMO based algorithms indexed by $i = 1, \dots, n$, where the update of the i-th algorithm is defined by*

$$\boldsymbol{X}^{t+1} - \boldsymbol{X}^{t} = \gamma_t \mathrm{LMO}_i(\boldsymbol{M}^t)\,,$$

and LMO_i *corresponds to the unit ball of norm $\|\cdot\|_i$. For arbitrary non-negative $\alpha_1, \dots, \alpha_n$, the algorithm with the update given by*

$$\boldsymbol{X}^{t+1} - \boldsymbol{X}^{t} = \gamma_t \sum_{i=1}^{n} \alpha_i \mathrm{LMO}_{\|\cdot\|_{(i)}}(\boldsymbol{M}^t)$$

is an LMO-algorithm itself, with LMO corresponding to the unit ball of the norm $\|\cdot\|$ dual to the norm given by $\sum_{i=1}^{n} \alpha_i \|\cdot\|_{(i)}^{\dagger}$.

4.2. Frobeniusize Them: F-Muon and F-Neon

We now construct concrete examples of algorithms obtained via linear combinations of LMO-algorithms. By Corollary 5, these combinations are themselves LMO-algorithms.

Combining Fanion-k with NSGD yields a family of algorithms with updates

$$\boldsymbol{X}^{t+1} = \boldsymbol{X}^{t} - \gamma_t \left(\alpha \sum_{i=1}^{k} \boldsymbol{u}_i \boldsymbol{v}_i^{\top} + (1-\alpha) \frac{\boldsymbol{M}^t}{\|\boldsymbol{M}^t\|_{\mathrm{F}}} \right). \tag{11}$$

Recall that Fanion-k operates under the dual to the Ky Fan k-norm, while NSGD operates under the self-dual Frobenius norm. By Corollary 5, this combination defines an LMO-algorithm with norm $\|\cdot\|_{\mathrm{F-KF-k}}^{\dagger}$, where

$$\|\cdot\|_{\mathrm{F-KF-k}} = \alpha \|\cdot\|_{\text{KF-}k} + (1-\alpha)\|\cdot\|_{\mathrm{F}}\,. \tag{12}$$

We call this family *F-Fanions.*

The extremal members of this family are *F-Neon* (with $k = 1$) and *F-Muon* (with $k = \min\{m, n\}$). Additional information and visualizations for the $\|\cdot\|_{\mathrm{F}*} = \|\cdot\|_{\mathrm{F-KF-1}}$ norm appear in the appendix (see Equation (17), Figure 7(a)subfigure).

4.3. Add SignSGD: S-Muon and S-Neon

Similarly, combining Fanion-k with SignSGD yields *S-Fanion-k* with update

$$\boldsymbol{X}^{t+1} = \boldsymbol{X}^{t} - \gamma_t \left(\alpha \sum_{i=1}^{k} \boldsymbol{u}_i \boldsymbol{v}_i^{\top} + (1-\alpha)\eta \operatorname{sign}(\boldsymbol{M}^t) \right), \tag{13}$$

where η is a scaling coefficient specific to SignSGD.

By Corollary 5, this defines an LMO-algorithm with norm $\|\cdot\|_{\mathrm{C-KF-k}}^{\dagger}$, where

$$\|\cdot\|_{\mathrm{C-KF-k}} = \alpha \|\cdot\|_{\text{KF-}k} + \frac{1-\alpha}{\eta} \|\cdot\|_{\mathrm{C}}^{\dagger}\,. \tag{14}$$

The extremal members of this family are *S-Neon* (with $k = 1$) and *S-Muon* (with $k = \min\{m, n\}$).

5. Computing the Updates

We employ the thick-restarted Lanczos method for the symmetric eigenvalue problem (thick-restart Lanczos, TRLan) to compute the low-rank updates of Fanions. We apply TRLan to either $\boldsymbol{M}^{t\top}\boldsymbol{M}^t$ or $\boldsymbol{M}^t\boldsymbol{M}^{t\top}$ (whichever matrix is smaller). We use the CuPy implementation of `cupy.sparse.linalg.svds` (Preferred Infrastructure and Developers, 2025) which internally relies on TRLan (Simonz, 1998).

TRLan is specifically designed for efficiently approximating the largest singular values and corresponding singular vectors of very large matrices. The thick-restart strategy retains the most informative Ritz vectors across restarts, which dramatically accelerates convergence while keeping memory consumption moderate. TRLan is particularly attractive in our GPU setting because its dominant cost is a modest number of highly parallelizable matrix-vector multiplications (matvecs) and it avoids full reorthogonalization against the entire Krylov basis by using short recurrence relations combined with thick restarting.

The per-cycle complexity is $\mathcal{O}(mn^2 + n^2k + nk^2)$, where $m \geq n$ are the dimensions of the target matrix and k is the size of the retained subspace (typically $k \ll n$).

In Table 1, we compare TRLan against randomized SVD (RSVD) and simple power iterations when computing the rank-k update used in Fanion-k and related algorithms. Experiments are performed on dense random matrices with i.i.d. $\mathcal{N}(0,1)$ entries and use CPU implementations for fair comparison. We report:

- err_1: relative error in the Frobenius norm of $\sum_i^k \boldsymbol{u}_i\boldsymbol{v}_i^T$,
- err_2: relative error in the Frobenius norm of $\sum_i^k \sigma_i\boldsymbol{u}_i\boldsymbol{v}_i^T$.

On 500×500 matrices, TRLan and RSVD require comparable wall-clock time, but TRLan delivers orders-of-magnitude lower error and far fewer matvecs. On larger 5000×5000 matrices the advantage becomes even more pronounced: TRLan is 3-4 times faster than RSVD while using ~30 times fewer matvecs at comparable or better accuracy.

An interesting empirical observation is that RSVD tends to approximate the *singular values* themselves reasonably well but the reconstructed low-rank matrix noticeably deviates from the truncated SVD, whereas TRLan provides an excellent approximation to the truncated SVD matrix itself (low err_2) at the cost of occasionally less accurate individual singular values. This makes TRLan the preferred choice for algorithms like Neon/Fanion-k that only need the low-rank term $\sum \sigma_i\boldsymbol{u}_i\boldsymbol{v}_i^\top$, but less ideal for methods (e.g., Dion) that explicitly require accurate σ_i for error feedback or step-size control.

A current practical limitation is the lack of a native PyTorch implementation of thick-restart Lanczos; existing PyTorch-based randomized SVD routines cannot match TRLan's accuracy/efficiency combination for the matrix reconstruction task.

For reference, Table 2 shows results for the Newton-Schulz polar decomposition iteration on the same matrices, err_1 is the relative error of $\boldsymbol{U}\boldsymbol{V}^T$ (29-30 iterations to converge, significantly higher matvec count than TRLan).

Table 1: Comparison of methods for computing rank-k updates on dense random matrices (CPU, double precision). Lower is better in all columns.

Matrix sizes	k	Method	Time (s)	Matvecs	Iterations	err_1	err_2
500×500	5	Power Iterations	0.062	2005	200	$9.2{\cdot}10^{-3}$	$9.1{\cdot}10^{-3}$
500×500	5	RSVD	0.017	1170	38	$9.8{\cdot}10^{-3}$	$9.6{\cdot}10^{-3}$
500×500	5	TRLan	0.018	131	65	$9.6{\cdot}10^{-5}$	$9.4{\cdot}10^{-5}$
500×500	50	Power Iterations	0.44	43750	437	$9.9{\cdot}10^{-3}$	$9.0{\cdot}10^{-3}$
500×500	50	RSVD	0.61	6120	50	$9.9{\cdot}10^{-3}$	$9.1{\cdot}10^{-3}$
500×500	50	TRLan	0.16	462	231	$3.3{\cdot}10^{-7}$	$3.0{\cdot}10^{-7}$
5000×5000	5	Power Iterations	9.6	9065	906	$8.6{\cdot}10^{-3}$	$8.6{\cdot}10^{-3}$
5000×5000	5	RSVD	2.1	5640	187	$9.7{\cdot}10^{-3}$	$9.7{\cdot}10^{-3}$
5000×5000	5	TRLan	0.70	205	102	$7.7{\cdot}10^{-3}$	$7.7{\cdot}10^{-3}$

Table 2: Newton-Schulz iterations on the same matrices (for reference).

Matrix size	Time (s)	Matvecs	Iterations	err_1
500×500	0.041	27 000	27	4.8e-3
5000×5000	26.4	290 000	29	6.5e-3

6. Experiments

6.1. Randomized Linear Least Squares

First, we compare F-Fanions on the following convex L-smooth problem:

$$F(\boldsymbol{X}) = \frac{1}{2}\langle(\boldsymbol{X} - \boldsymbol{S}), \boldsymbol{M}(\boldsymbol{X} - \boldsymbol{S})\boldsymbol{N}\rangle \to \min_{\boldsymbol{X} \in \mathbb{R}^{m \times n}} \tag{15}$$

where $\boldsymbol{X} \in \mathbb{R}^{m \times n}$, $m = 500$ and $n = 500$ are typical dimensions of a neural network weight matrix, $\boldsymbol{S} \in \mathbb{R}^{m \times n}$, $\boldsymbol{M} \in \mathbb{S}^m_+$ and $\boldsymbol{N} \in \mathbb{S}^n_+$ are positive-semidefinite matrices. The spectra of $\boldsymbol{M}$ and $\boldsymbol{N}$ are uniformly distributed in the $(0, 1)$ interval. We set $\boldsymbol{S} = 0$, and $\boldsymbol{X}^0 \sim 0.1\mathcal{N}(0, \boldsymbol{I})$.

We run different Fanions and their respective F-Fanions with $\alpha = 1/2$: Neon (Fanion-1), Fanion-2, Fanion-10, Fanion-100, and Muon (Fanion-500). Also, we test S-Fanions with $\alpha = 1/2$ and `sign_lr_coeff=0.01`. We test them against Normalized SGD and SignSGD, which are also F-Fanion and S-Fanion respectively with $\alpha = 0$ and an arbitrary k.

Since theoretical bounds (Kovalev, 2025; Riabinin et al., 2025) rely on a very loose norm bound $\|\cdot\| \leq \rho\|\cdot\|_{\mathrm{F}}$, we do not derive learning rate or Nesterov momentum from the smoothness constants that also depend on the norm choice. Rather, we find such `(lr, momentum)` pair that the loss threshold 0.001 is reached in a minimal number of iterations. This setting is the most realistic, and at the same time aligns with the corollaries of the convergence theorems where constant learning rate and momentum coefficients are proposed.

We perform a grid search for `momentum` $\in \{0.1, 0.2, 0.3, 0.4, 0.5, 0.6, 0.7, 0.8, 0.9, 0.95\}$ and for `lr`. For Muon's, F-Muon's, S-Muon's `lr` $\in [0.005, 0.0020]$. For SignSGD, `lr` $\in 0.01 \times [0.005, 0.020]$, and for NSGD `lr` $\in [0.01, 0.10]$. The tuned parameters and the number of iterations to converge to 0.001 are in Table 3. `lr` and `momentum`, and `sign_lr_coeff` for Fanions, F-Fanions, and S-Fanions are the same as for Muon, F-Muon, and S-Muon respectively due to the impossibility to tune them properly: their losses decrease too slow to reach 0.001.

The results are presented in Figure 1 and detailed in Section E.

Both F-Muon and S-Muon converge faster and to a lower loss and a lower Frobenius norm of the gradient than NSGD, Muon, or SignSGD.

Table 3: Tuning learning rates and momentum coefficients

Algorithm	`lr`	`momentum`	Iterations to 0.001 loss
Muon	0.007	0.5	1060
NSGD	0.08	0.95	1020
F-Muon	0.015	0.7	910
SignSGD	0.016×0.01	0.95	2650
S-Muon	0.011	0.9	890

6.2. CIFAR-10 airbench

We compare the algorithms on the CIFAR-10 airbench (Keller, 2023). First, to test the impact of α, we run F-Muon for different α with the same `lr=0.24(1 - step/total_steps), momentum=0.65, nesterov=True` and weight normalization, as have been finetuned by Keller Jordan, 10 repetitions for each α. We record the accuracy after 8 epochs of training (Figure 2(a)subfigure).

Then we tune F-Muon with $\alpha = 0.5$. Tuned parameters are `lr=0.4(1 - step/total_steps), momentum=0.6, nesterov = True`. Tuned F-Muon reaches $94.02 \pm 0.13\%$ after 8 epochs (averaged by 200 iterations), matching Muon's accuracy and variance. Once again we measure `val_accuracy`(α) curve (Figure 2(b)subfigure). We notice that even when $\alpha = 0.1$, the accuracy is much higher than in the case of vanilla NSGD.

We tune S-Muon with $\alpha = 0.5$ for the best `(lr, momentum, sign_lr_coeff)` and by setting `lr=0.42(1 - step/total_steps), momentum=0.63, nesterov = True, sign_lr_coeff = 0.003` get **94.03** $\pm\, 0.13\%$, which is even higher than for vanilla Muon.

The Muon-level performance is surprising for the contorted geometry of F-Muon and S-Muon. F-Muon can be visualized by Figure 3, where the LMO balls of Muon and F-Muon for real `lr` are plotted in a 2D space of singular values. S-Muon cannot be visualized because the l_∞ norm is not a function of singular values, while $\|\cdot\|_2$, when plotted for the $\mathbb{R}^{m\times n}$ space with $m, n > 2$, requires at least a 4D space. However, it is plain that the LMO ball of S-Muon significantly differs from the ball of Muon because the `lr`$(1-\alpha)$`sign_lr_coeff` $= 6.3 \times 10^{-4}$, which is comparable to the usual `lr` of SignSGD for deep learning problems.

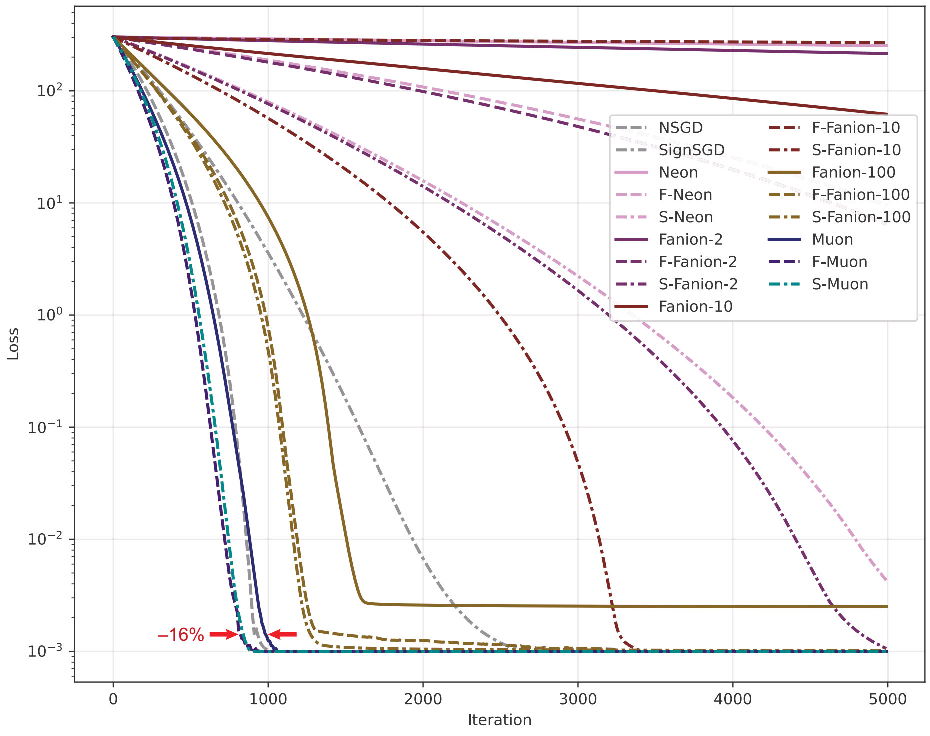

(a) The loss

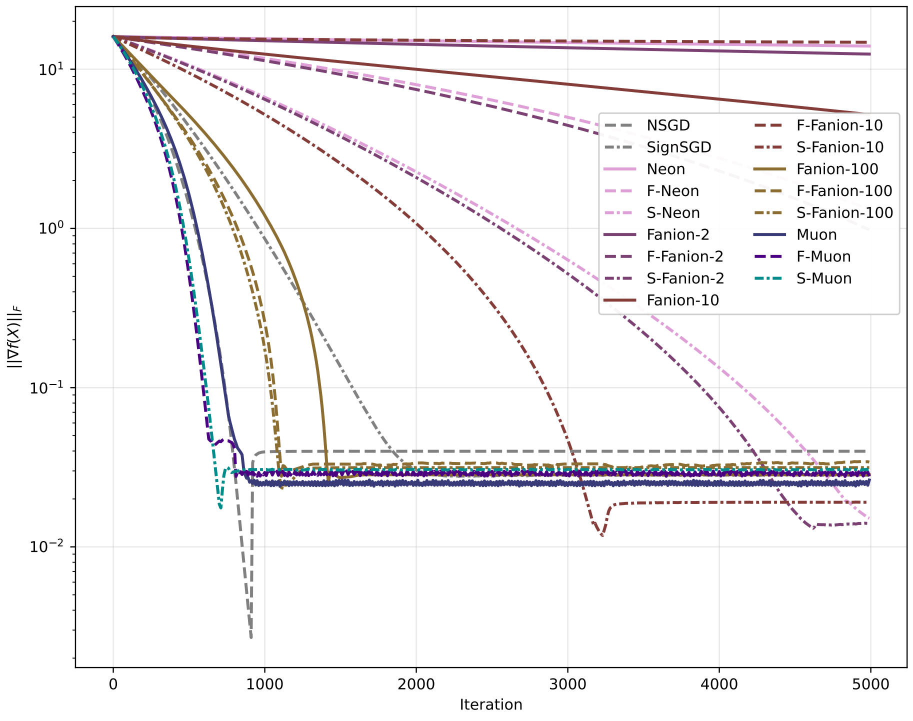

(b) The Frobenius norm of the gradient

Figure 1: Linear least squares problem for a 500x500 matrix

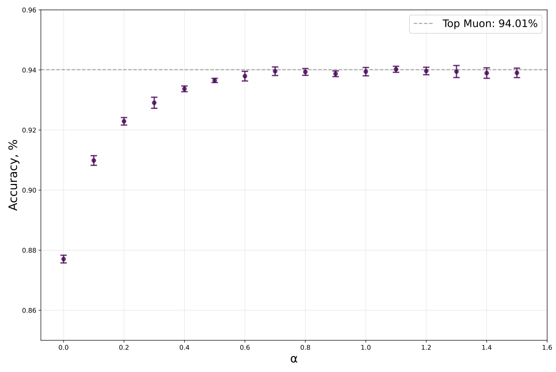

(*a*) With parameters tuned for Muon

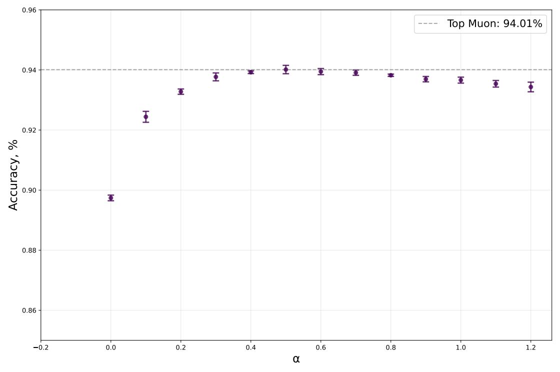

(*b*) With parameters tuned for F-Muon

Figure 2: Mean validation accuracies for F-Muon with different α

The most pathological case is $\alpha > 1$, which corresponds to the LMO with an area that is not a norm ball! Despite this violation, the mixture of algorithms reaches almost the same accuracy as vanilla Muon.

These observations raise the question of how much LMO-based algorithms are sensitive to the constraint area.

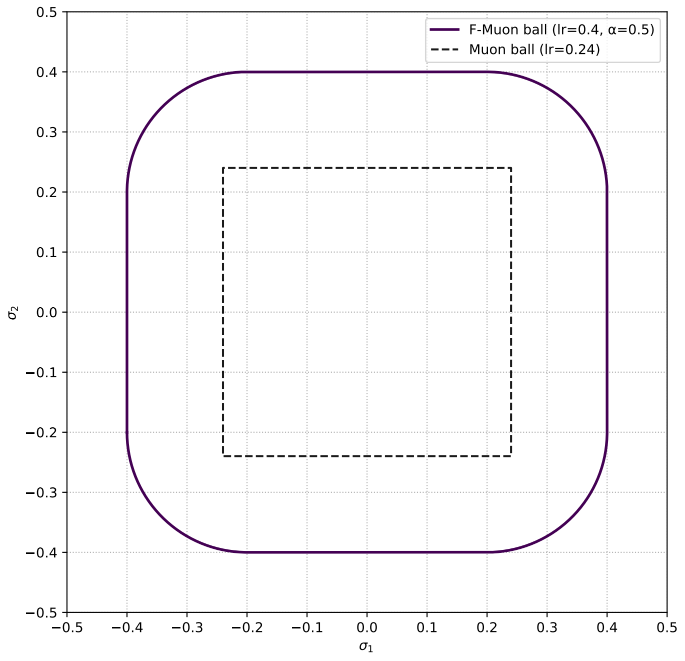

Figure 3: Visualization of the LMO balls for Muon and F-Muon.

6.3. NanoGPT speedrun

We test F-Muon on the NanoGPT speedrun (Jordan et al., 2024a). For $\alpha = 0.5$, the optimal parameters are `lr=0.07, momentum=0.95`, while for Muon they were `lr=0.05, momentum=0.95`. After testing for 1750 steps we get 3.281 cross-entropy loss. For Muon, it falls below the target threshold 3.28 and reaches 3.279. However, this difference is negligible if one looks at Figure 4. It is even more striking, considering the fact that this F-Muon is an average of Muon and NSGD, and the latter performed quite poorly.

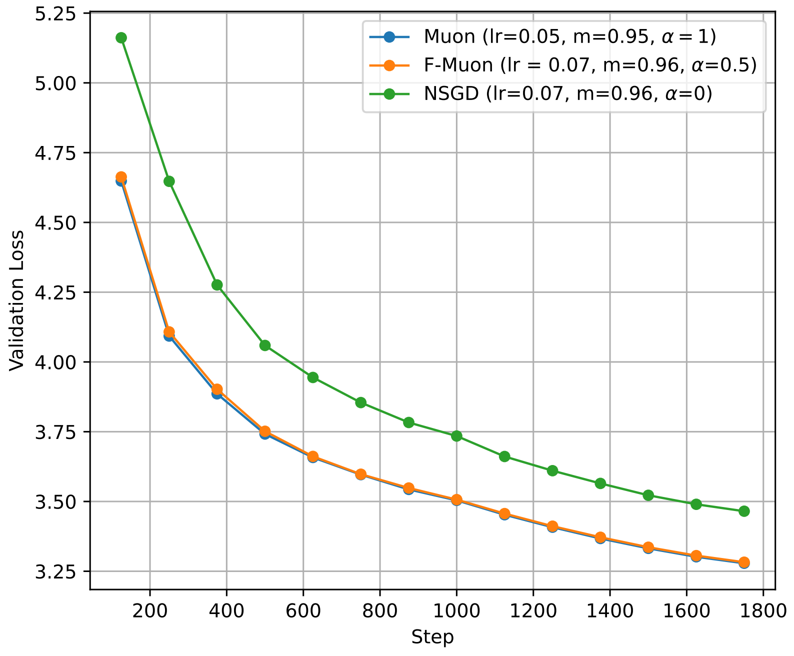

Figure 4: The validation loss for NanoGPT

Again, as on the CIFAR airbench, if we set $\alpha = -0.1$ that corresponds to no ball, we get a 3.2818 loss, which is a small difference from the baseline.

6.4. NanoGPT Fine-Tuning

We fine-tuned the NanoGPT framework by Karpathy (Karpathy, 2022) using the standard *NanoGPT-medium* configuration, which corresponds to GPT-2 Medium. This model consists of 24 transformer layers, a hidden size of 1024, 16 attention heads, and approximately 345 million parameters. The training dataset was the *Tiny Stories* corpus (Eldan and Li, 2023), selected for its high entropy and structural diversity, which amplify and make more visible the differences in optimization dynamics. All training runs were initialized with the same random seed, weight initialization, and learning rate schedule to ensure that any differences in performance arose solely from the choice of optimizer.

For all one-dimensional layers, AdamW was used with a learning rate of 1×10^{-3}. Since momentum exhibited negligible influence on training dynamics, it was held constant across all experiments. A comparative analysis of optimization performance is provided in Figure 5.

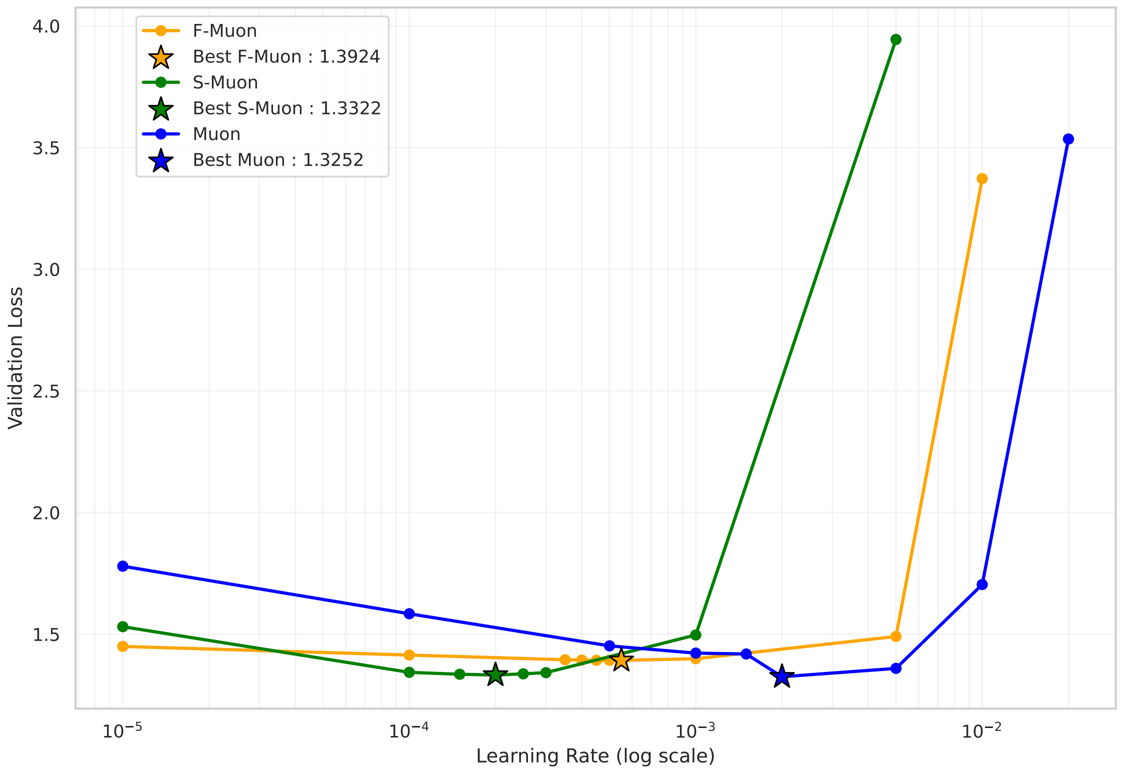

Figure 5: Comparison of Muon, F-Muon, and S-Muon across a range of learning rates. Stars denote the best learning rate identified for each optimizer. Validation loss.

Figure 6 presents the train and validation loss curves at the optimal learning rate for each optimizer. While F-Muon and S-Muon maintain consistent behavior, vanilla Muon attains the lowest loss overall.

7. Algorithms for Vectors $\rightarrow$ Algorithms for Matrices

One cannot but notice the similarity between the updates of LMO optimizers in the vector l_p and the matrix Schatten S_p norms, which is illustrated by Table 4. The parallels are not limited to mere similarity of the updates and can be traced even in the empirical observations. SignSGD is very close to Adam, as noted in (Bernstein and Newhouse, 2024), and both Adam and Muon perform well in training large models (Zhao et al., 2025; Liu et al., 2025). NSGD is the same for both matrix and vector cases. Greedy Coordinate

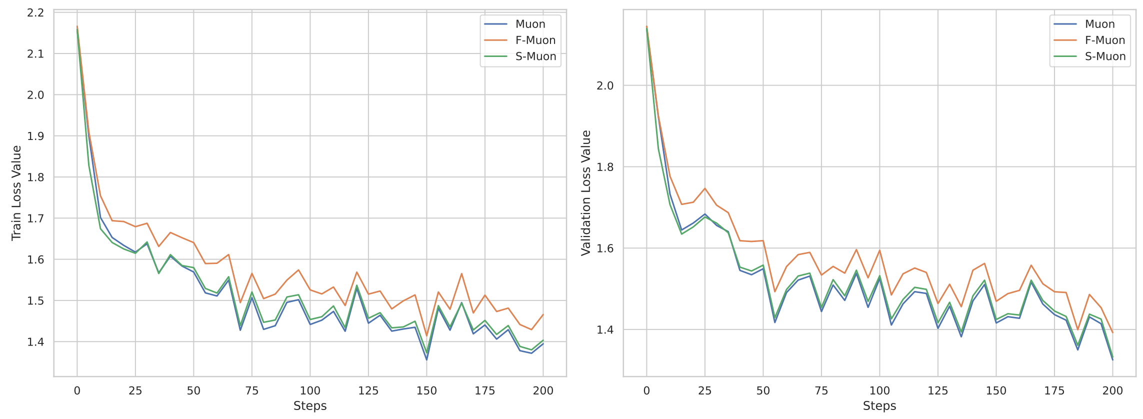

Figure 6: Train and validation loss at the optimal learning rate for each optimizer. The standard Muon method achieves the lowest loss, while F-Muon and S-Muon remain stable but exhibit slightly inferior performance.

Table 4: LMO optimizers in Schatten S_p norms and in l_p norms. g is the gradient. When it is a matrix, $g = \boldsymbol{U}\boldsymbol{\Sigma}\boldsymbol{V}^\top$

Algorithm	LMO constraint set $\mathcal{D}$	LMO	Reference
Normalized SGD	l_2-ball, S_2-ball	$-\eta\frac{g}{\|g\|_2} = -\eta\frac{g}{\|g\|_{\mathrm{F}}}$	(Hazan et al., 2015)
Momentum Normalized SGD	Ball in l_2, or Ball in S_2	$-\eta\frac{g}{\|g\|_2} = -\eta\frac{g}{\|g\|_{\mathrm{F}}}$	(Cutkosky et al., 2020)
SignSGD	Ball in Max-norm l_∞	$-\eta\,\mathrm{sign}(g)$	(Bernstein et al., 2018, Thm. 1)
Signum	Ball in Max-norm l_∞	$-\eta\,\mathrm{sign}(g)$	(Bernstein et al., 2018, Thm. 3)
Muon	Ball in Spectral S_∞	$-\eta\boldsymbol{U}\boldsymbol{V}^\top$	(Jordan et al., 2024b)
Gauss-Southwell Coordinate Descent	Ball in l_1	$-\eta\sum_{i\in\arg\max\|g_i^t\|}\mathrm{sign}(g_i^t)e_i$	(Shi et al., 2016, p. 19)
Neon	Ball in Nuclear S_1	$-\eta\boldsymbol{u}_1\boldsymbol{v}_1^\top$	This work

Descent is not applied to high-dimensional problems, so from this perspective it is not surprising that one-rank Neon underperforms on such problems.

8. Related Work and Discussion

Since Muon (Jordan et al., 2024b) is a very efficient optimizer for functions of weight matrices, a lot of research has been put into, first, further improving its performance, and second, explaining its success.

Improvements of Muon Regarding the first point, a large number of applications and improvements of Muon has been proposed in less than a year. (Liu et al., 2025) adapted the algorithm for training language models larger than NanoGPT. (Shah et al., 2025) organized efficient hyperparameter transfer by combining Muon with maximal update parametrization. To construct their COSMOS optimizer, (Chen et al., 2025) applied computationally intensive updates of SOAP optimizer (Vyas et al., 2025) to a low-dimensional "leading eigensubspace" while using memory-efficient methods like Muon for the remaining parameters. (Amsel et al., 2025; Grishina et al., 2025) proposed more efficient alternatives to Newton-Schulz algorithm. (Si et al., 2025) introduced AdaMuon which combines element-wise adaptivity with orthogonal updates. We suppose that the described above or similar techniques can be applied to our optimizers as well. For example, F-Muon and S-Muon also benefit from faster alternatives to Newton-Schulz iterations, and Fanions may be a great substitute to Muon in COSMOS, because, as we have shown in Section 5, Lanczos algorithm is much faster than Newton-Schulz iterations on very large matrices.

Theory behind Muon Regarding the second point, there has been a prolonged gap in theory behind Muon, simplistic derivation of (Bernstein, 2025) based on (Bernstein and Newhouse, 2024) excluded. This gap, as it seems to us, is not even now completely closed. For example, (Kovalev, 2025) has provided convergence guarantees of Muon and in various settings, from which, however, Muon's supremacy cannot be recovered. Indeed, although the obtained bounds depend on the norm choice, the asymptotics of the convergence remain the same as for NSGD and other optimizers, $K = \mathcal{O}(\varepsilon^{-4})$ in an L-smooth stochastic case.

A similar drawback has the article (Riabinin et al., 2025), where L-smoothness assumption is replaced with a more practical (L_0, L_1)-smoothness. By estimating smoothness and substituting it into their Theorem 1, the authors recovered the optimal fine-tuned stepsizes reported by (Pethick et al., 2025c). However, they have not showed the optimality of the spectral or the RMS-to-RMS norm, which is observed in practice, as our comparison with NSGD highlights.

Common important drawback of the analyses is the consideration of the convergence by the norm of the gradient. As we showed in our experiments on CIFAR, the gradient norm may decrease only by a factor of ten, when the accuracy reaches 100%.

We suppose that the reason for the recorded stark discrepancy between Neon and Muon performance, both of which are described by Stochastic Conditional Gradient (Pethick et al., 2025c) or Gluon frameworks, lies in the structure of the norm ball or in the preconditioner interpretation (Pethick et al., 2025a), which must be an object of further research.

The LMO and Error Feedback We already mentioned that rank-k unsharded Dion without error feedback and scaling of the update is Fanion-k. Since error feedback for Dion is very important as discovered by the ablation study in (Ahn et al., 2025), F-Fanions and S-Fanions will benefit from it as well. In the context of federated learning, error feedback is effective even for compressed Muon (Gruntkowska et al., 2025a). The advantage of Fanions and S-Fanions is that less bits are required for transmission: $\sum_{i=1}^{k} \boldsymbol{u}_i \boldsymbol{v}_i^\top$ is easily transmitted as $\{\boldsymbol{u}_1, \boldsymbol{v}_1, \ldots, \boldsymbol{u}_k, \boldsymbol{v}_k\}$ ($(m+n) \times k$ floats), while the sign part is as usual coded in $m \times n$ bits. Thus, the compression is "built-in". Moreover, there is an intriguing possibility to construct differentially private Fanions and S-Fanions with the specific more optimal non-Gaussian noise, as was done with DP-signSGD (Jang et al., 2024). This we leave for future research.

The nuclear norm in the LMO As we found out only when transforming our results into an article, the nuclear norm has already been explored in the context of the linear minimization oracle. (Pethick et al., 2025b) applied it to create νSAM, a new sharpness-aware minimization technique. It would be interesting to substitute $\|\cdot\|_*$ with $\|\cdot\|^\dagger_{\text{KF-}k}$ in their approach. Since the SAM-neighborhood becomes more diverse, $k > 1$ might add to the accuracy boost, while preserving a small memory footprint and a small time overhead, if Dion-style power iterations are used.

Orthogonal research Fanions, F-Fanions, and S-Fanions benefit from the general theoretical description of (Riabinin et al., 2025), and better learning rates can be predicted by calculating the trajectory smoothness. They could be transformed to Drop-Fanions by updating only some layers as in (Gruntkowska et al., 2025b). They could be viewed as approximations of the Non-Euclidean Broximal Point Method for the corresponding norms (Gruntkowska and Richtárik, 2025). One can clip them to produce ClippedScion-like algorithms (Pethick et al., 2025d). They could be made more memory-effective by the zero-order techniques that worked for Muon (Petrov et al., 2025). Finally, the results from (Shulgin et al., 2025) can be used to explain the robustness of Muon to the norm change that occurred in our experiments and to theoretically derive faster yet working approximate schemes to calculate the LMO; power iterations with a very limited number of iterations is a good algorithm to consider for the analysis.

9. Conclusion

In this article, we have generalized several successful algorithms, like Muon, Dion and νSAM, to the LMO-based algorithms in the $\|\cdot\|^\dagger_{\text{KF-}k}$ norm. Also we have proposed the technique of “regularizing” the updates with NSGD or SignSGD, a trick to increase the robustness of the algorithms, which is motivated by the consideration of the $\|\cdot\|_{\mathrm{F-KF-k}}$ and $\|\cdot\|_{\mathrm{C^\dagger-KF-k}}$ norms. We suggest that future works that deal with the non-Euclidean LMO explain in the corollaries to their convergence theorems the empirical superiority of Muon to other Fanions, and ideally accont for S-Fanion and F-Muon robustness as well. Without that, it is hard to believe that the bounds are relevant for practitioners, as we see by the notorious example of one-rank Neon.

10. Author Contributions

IO suggested using the nuclear norm in the (Bernstein and Newhouse, 2024) framework. DM presented the problem at the MIPT optimization course. IK suggested using composite norms (though not the ones that induce F-Fanions and S-Fanions) and refactored Section 4. NK suggested Lanczos algorithm as the most precise means to compute Fanions' updates, conducted experiments to prove this, and wrote Section 5. AV conducted the finetuning of NanoGPT on Tiny Stories and wrote Section 6.4. All other work was done by AK: constructing Fanions, F-Fanions, S-Fanions, experimenting on the Linear Least Squares, CIFAR-airbench and NanoGPT pretrain, and writing the manuscript.

References

Kwangjun Ahn, Byron Xu, Natalie Abreu, Ying Fan, Gagik Magakyan, Pratyusha Sharma, Zheng Zhan, and John Langford. Dion: Distributed orthonormalized updates, 2025. URL https://arxiv.org/abs/2504.05295.

Noah Amsel, David Persson, Christopher Musco, and Robert M Gower. The polar express: Optimal matrix sign methods and their application to the muon algorithm. *arXiv preprint arXiv:2505.16932*, 2025.

Jeremy Bernstein. Deriving muon, 2025. URL https://jeremybernste.in/writing/deriving-muon.

Jeremy Bernstein and Laker Newhouse. Old optimizer, new norm: An anthology. *arXiv preprint arXiv:2409.20325*, 2024.

Jeremy Bernstein, Yu-Xiang Wang, Kamyar Azizzadenesheli, and Animashree Anandkumar. signsgd: Compressed optimisation for non-convex problems. In *International conference on machine learning*, pages 560–569. PMLR, 2018.

Rajendra Bhatia. *Matrix analysis*, volume 169. Springer Science & Business Media, 2013.

Franz Louis Cesista. Steepest Descent under Schatten-p Norms, February 2025. URL https://leloykun.github.io/ponder/steepest-descent-schatten-p/.

Weizhu Chen, Chen Liang, Tuo Zhao, Zixuan Zhang, Hao Kang, Liming Liu, Zichong Li, and Zhenghao Xu. Cosmos: A hybrid adaptive optimizer for memory-efficient training of llms, 2025. URL https://arxiv.org/abs/2502.17410.

Ashok Cutkosky, Harsh Mehta, and Francesco Orabona. Momentum-based variance reduction in nonconvex sgd. *Advances in Neural Information Processing Systems*, 2020.

Ronen Eldan and Yuanzhi Li. Tinystories: How small can language models be and still speak coherent english?, 2023. URL https://arxiv.org/abs/2305.07759.

Ekaterina Grishina, Matvey Smirnov, and Maxim Rakhuba. Accelerating newton-schulz iteration for orthogonalization via chebyshev-type polynomials, 2025. URL https://arxiv.org/abs/2506.10935.

Kaja Gruntkowska and Peter Richtárik. Non-euclidean broximal point method: A blueprint for geometry-aware optimization, 2025. URL https://arxiv.org/abs/2510.00823.

Kaja Gruntkowska, Alexander Gaponov, Zhirayr Tovmasyan, and Peter Richtárik. Error feedback for muon and friends, 2025a. URL https://arxiv.org/abs/2510.00643.

Kaja Gruntkowska, Yassine Maziane, Zheng Qu, and Peter Richtárik. Drop-muon: Update less, converge faster, 2025b. URL https://arxiv.org/abs/2510.02239.

Elad Hazan, Kfir Levy, and Shai Shalev-Shwartz. Beyond convexity: Stochastic quasi-convex optimization. *Advances in neural information processing systems*, 28, 2015.

Jonggyu Jang, Seongjin Hwang, and Hyun Jong Yang. Rethinking DP-SGD in discrete domain: Exploring logistic distribution in the realm of signSGD. In Ruslan Salakhutdinov, Zico Kolter, Katherine Heller, Adrian Weller, Nuria Oliver, Jonathan Scarlett, and Felix Berkenkamp, editors, *Proceedings of the 41st International Conference on Machine Learning*, volume 235 of *Proceedings of Machine Learning Research*, pages 21241–21265. PMLR, 21–27 Jul 2024. URL https://proceedings.mlr.press/v235/jang24a.html.

Keller Jordan, Jeremy Bernstein, Brendan Rappazzo, @fernbear.bsky.social, Boza Vlado, You Jiacheng, Franz Cesista, Braden Koszarsky, and @Grad62304977. modded-nanogpt: Speedrunning the nanogpt baseline, 2024a. URL https://github.com/KellerJordan/modded-nanogpt.

Keller Jordan, Yuchen Jin, Vlado Boza, Jiacheng You, Franz Cesista, Laker Newhouse, and Jeremy Bernstein. Muon: An optimizer for hidden layers in neural networks, 2024b. URL https://kellerjordan.github.io/posts/muon/.

Andrej Karpathy. nanogpt: The simplest, fastest repository for training/finetuning medium-sized gpts. GitHub repository, 2022. URL https://github.com/karpathy/nanoGPT.

Jordan Keller. cifar10-airbench, 2023. URL https://github.com/KellerJordan/cifar10-airbench.

Diederik P Kingma and Jimmy Ba. Adam: A method for stochastic optimization. *arXiv preprint arXiv:1412.6980*, 2014.

Dmitry Kovalev. Understanding gradient orthogonalization for deep learning via non-euclidean trust-region optimization. *arXiv preprint arXiv:2503.12645*, 2025.

Dmitry Kovalev and Ekaterina Borodich. Non-euclidean sgd for structured optimization: Unified analysis and improved rates, 2025. URL https://arxiv.org/abs/2511.11466.

Jingyuan Liu, Jianlin Su, Xingcheng Yao, Zhejun Jiang, Guokun Lai, Yulun Du, Yidao Qin, Weixin Xu, Enzhe Lu, Junjie Yan, et al. Muon is scalable for llm training. *arXiv preprint arXiv:2502.16982*, 2025.

Ilya Loshchilov and Frank Hutter. Decoupled weight decay regularization. *arXiv preprint arXiv:1711.05101*, 2017.

Thomas Pethick. Understanding dion, 2025. URL https://pethick.dk/posts/2025-08-18-understanding-dion/.

Thomas Pethick, Kimon Antonakopoulos, Antonio Silveti-Falls, Leena Chennuru Vankadara, and Volkan Cevher. Training neural networks at any scale, 2025a. URL https://arxiv.org/abs/2511.11163.

Thomas Pethick, Parameswaran Raman, Lenon Minorics, Mingyi Hong, Shoham Sabach, and Volkan Cevher. νSAM: Memory-efficient sharpness-aware minimization via nuclear norm constraints. *Transactions on Machine Learning Research*, 2025b. ISSN 2835-8856. URL https://openreview.net/forum?id=V6ia5hWIMD.

Thomas Pethick, Wanyun Xie, Kimon Antonakopoulos, Zhenyu Zhu, Antonio Silveti-Falls, and Volkan Cevher. Training deep learning models with norm-constrained lmos. *arXiv preprint arXiv:2502.07529*, 2025c.

Thomas Pethick, Wanyun Xie, Mete Erdogan, Kimon Antonakopoulos, Tony Silveti-Falls, and Volkan Cevher. Generalized gradient norm clipping & non-euclidean (l_0, l_1)-smoothness, 2025d. URL https://arxiv.org/abs/2506.01913.

Egor Petrov, Grigoriy Evseev, Aleksey Antonov, Andrey Veprikov, Nikolay Bushkov, Stanislav Moiseev, and Aleksandr Beznosikov. Leveraging coordinate momentum in signsgd and muon: Memory-optimized zero-order, 2025. URL https://arxiv.org/abs/2506.04430.

Inc. Preferred Infrastructure and CuPy Developers. CuPy: `cupyx.scipy.sparse.linalg.svds` — api reference. https://docs.cupy.dev/en/stable/reference/generated/cupyx.scipy.sparse.linalg.svds.html, 2025. Accessed: 2025-08-24.

Artem Riabinin, Egor Shulgin, Kaja Gruntkowska, and Peter Richtárik. Gluon: Making muon & scion great again!(bridging theory and practice of lmo-based optimizers for llms). *arXiv preprint arXiv:2505.13416*, 2025.

Ishaan Shah, Anthony M Polloreno, Karl Stratos, Philip Monk, Adarsh Chaluvaraju, Andrew Hojel, Andrew Ma, Anil Thomas, Ashish Tanwer, Darsh J Shah, et al. Practical efficiency of muon for pretraining. *arXiv preprint arXiv:2505.02222*, 2025.

Hao-Jun Michael Shi, Shenyinying Tu, Yangyang Xu, and Wotao Yin. A primer on coordinate descent algorithms. *arXiv preprint arXiv:1610.00040*, 2016.

Egor Shulgin, Sultan AlRashed, Francesco Orabona, and Peter Richtárik. Beyond the ideal: Analyzing the inexact muon update, 2025. URL https://arxiv.org/abs/2510.19933.

Chongjie Si, Debing Zhang, and Wei Shen. Adamuon: Adaptive muon optimizer. *arXiv preprint arXiv:2507.11005*, 2025.

Kesheng Wuzand Horst Simonz. Thick-restart lanczos method for symmetric eigenvalue problemsy. 1998.

Nikhil Vyas, Depen Morwani, Rosie Zhao, Mujin Kwun, Itai Shapira, David Brandfonbrener, Lucas Janson, and Sham Kakade. Soap: Improving and stabilizing shampoo using adam, 2025. URL https://arxiv.org/abs/2409.11321.

Yao-Liang Yu. Arithmetic duality for norms, 2012. URL https://cs.uwaterloo.ca/~y328yu/notes/normduality.pdf.

Rosie Zhao, Depen Morwani, David Brandfonbrener, Nikhil Vyas, and Sham M. Kakade. Deconstructing what makes a good optimizer for autoregressive language models. In *The Thirteenth International Conference on Learning Representations*, 2025. URL https://openreview.net/forum?id=zfeso8ceqr.

Appendix A. LMO for Neural Networks

In a typical neural network, the objective function F depends on a set of weight matrices $\{\boldsymbol{W}_1, \boldsymbol{W}_2, \ldots\}$. The optimization framework we have described is applied in a layer-wise fashion. At each iteration t, a stochastic gradient $g(\boldsymbol{X}^t, \xi^t)$ is computed using a mini-batch of data with the ξ^t noise via backpropagation. This yields a separate gradient component,

$\boldsymbol{G}_i^t$, for each matrix $\boldsymbol{X}_i$. The LMO-based update rule is then applied to each matrix $\boldsymbol{X}_i$ using its corresponding gradient component $\boldsymbol{G}_i^t$.

The update rule used in Muon optimizer is uSCG (Pethick et al., 2025c). In the most general case, which involves momentum, it can be written as

$$\begin{aligned} \boldsymbol{M}^t &= \alpha_t g(\boldsymbol{X}^t, \xi^t) + (1-\alpha_t)\boldsymbol{M}^{t-1}\,, \\ \boldsymbol{X}^{t+1} &= \boldsymbol{X}^t + \gamma_t \mathrm{LMO}(\boldsymbol{M}^t)\,. \end{aligned} \tag{16}$$

Appendix B. Norms $\|\cdot\|_{\mathrm{F}*}^{\dagger}$ and $\|\cdot\|_{\mathrm{F}2}^{\dagger}$

Based on the lemma, we immediately find $\|\cdot\|_{\mathrm{F}*}^{\dagger}$, which is related to F-Muon update. Indeed, after setting $\beta = 1-\alpha$ and remembering that for smooth and bounded cases we can use min instead of inf, we get

$$\|\boldsymbol{Y}\|_{\mathrm{F}*}^{\dagger} = \min_{\boldsymbol{Z}} \min_{t} \{t, s.t. \|\boldsymbol{Z}\|_2 \leq \alpha t, \|\boldsymbol{Y}-\boldsymbol{Z}\|_{\mathrm{F}} \leq (1-\alpha)t\} \tag{17}$$

If $\alpha = 1$, then $\boldsymbol{Z} = \boldsymbol{Y}$, and we get $\|\boldsymbol{Y}\|_{\mathrm{F}*}^{\dagger} = \|\boldsymbol{Y}\|_2$. If $\alpha = 0$, then $\boldsymbol{Z} = 0$, and we get $\|\boldsymbol{Y}\|_{\mathrm{F}*}^{\dagger} = \|\boldsymbol{Y}\|_{\mathrm{F}}$.

Similarly, we find $\|\cdot\|_{\mathrm{F}2}^{\dagger}$, which is related to F-Neon update:

$$\|\boldsymbol{Y}\|_{\mathrm{F}2}^{\dagger} = \min_{\boldsymbol{Z}} \min_{t} \{t, s.t. \|\boldsymbol{Z}\|_* \leq \alpha t, \|\boldsymbol{Y}-\boldsymbol{Z}\|_{\mathrm{F}} \leq (1-\alpha)t\} \tag{18}$$

If $\alpha = 1$, then $\boldsymbol{Z} = \boldsymbol{Y}$, and we get $\|\boldsymbol{Y}\|_{\mathrm{F}2}^{\dagger} = \|\boldsymbol{Y}\|_*$. If $\alpha = 0$, then $\boldsymbol{Z} = 0$, and we get $\|\boldsymbol{Y}\|_{\mathrm{F}2}^{\dagger} = \|\boldsymbol{Y}\|_{\mathrm{F}}$.

Unfortunately, $\|\cdot\|_{\mathrm{F}*}^{\dagger}$ and $\|\cdot\|_{\mathrm{F}2}^{\dagger}$ do not have a closed-form expression.

Appendix C. Proof of Lemma on Dual of Convex Combinations

We provide here the proof of Lemma 3.

Proof Let us first prove the lemma for the case $n = 2$. Denote $f(x) = \alpha_1\|x\|_{(1)}$ and $g(x) = \alpha_2\|x\|_{(2)}$, such that $\|x\| = f(x) + g(x)$. Recall two standard facts:

1. For any norm $\|\cdot\|$ and $\lambda > 0$,

$$(\lambda\|\cdot\|)^*(y) = \sup_x \big(\langle y, x\rangle - \lambda\|x\|\big) = \delta_{\lambda\mathcal{B}_{\|\cdot\|^\dagger}}(y)\,,$$

   i.e., the indicator function of the scaled dual ball.

2. The Fenchel conjugate of a sum satisfies

$$(f+g)^*(y) = \inf_{u+v=y} \big(f^*(u) + g^*(v)\big)\,.$$

Applying these to f and g, we have

$$f^*(u) = \delta_{\alpha_1\mathcal{B}_{\|\cdot\|_{(1)}^\dagger}}(u)\,, \quad g^*(v) = \delta_{\alpha_2\mathcal{B}_{\|\cdot\|_{(2)}^\dagger}}(v)\,.$$

Thus,

$$\|\cdot\|^*(y) = (f+g)^*(y) = \inf_{u+v=y}\left(\delta_{\alpha_1\mathcal{B}_{\|\cdot\|^\dagger_{(1)}}}(u) + \delta_{\alpha_2\mathcal{B}_{\|\cdot\|^\dagger_{(2)}}}(v)\right) = \delta_{\alpha_1\mathcal{B}_{\|\cdot\|^\dagger_{(1)}}+\alpha_2\mathcal{B}_{\|\cdot\|^\dagger_{(2)}}}(y).$$

By definition, the conjugate of a norm is exactly the indicator of its dual unit ball:

$$\|\cdot\|^*(y) = \delta_{\mathcal{B}_{\|\cdot\|^\dagger}}(y)\,.$$

Therefore, $\mathcal{B}_{\|\cdot\|^\dagger} = \alpha_1\mathcal{B}_{\|\cdot\|^\dagger_{(1)}} + \alpha_2\mathcal{B}_{\|\cdot\|^\dagger_{(2)}}$.

Now we prove the general case by induction. The base case ($n = 2$) is already proven. Suppose that the assumption of the lemma holds for $n = k$. Then, for $n = k+1$,

$$\|x\| = \sum_{i=1}^{k}\alpha_i\|x\|_{(i)} + \alpha_{k+1}\|x\|_{(k+1)} = \|x\|_{(1:k)} + \alpha_{k+1}\|x\|_{(k+1)}\,.$$

Applying the result for $n = 2$ combined with the induction assumption, we obtain

$$\mathcal{B}_{\|\cdot\|^\dagger} = \mathcal{B}_{\|\cdot\|^\dagger_{(1:k)}} + \alpha_{k+1}\mathcal{B}_{\|\cdot\|^\dagger_{(k+1)}} = \sum_{i=1}^{k+1}\alpha_i\mathcal{B}_{\|\cdot\|^\dagger_{(i)}}\,,$$

which proves the lemma. ■

Appendix D. Visualization of different matrix norms

D.1. Duals to F* and F2 norms

It follows from Lemma 3 that the norm ball in $\|\cdot\|^\dagger_{\mathrm{F}*}$ is the Minkowski sum of the norm ball in $\alpha\|\cdot\|_*$ and $(1-\alpha)\|\cdot\|_{\mathrm{F}}$ and the norm ball in $\|\cdot\|^\dagger_{\mathrm{F}2}$ is the Minkowski sum of the norm ball in $\alpha\|\cdot\|_2$ and $(1-\alpha)\|\cdot\|_{\mathrm{F}}$.

In Figure 7 we plot these norms. On x-axis and y-axis, there are singular values σ_1, σ_2 respectively of a matrix from $\mathbb{R}^{m\times n}$ with $\min\{m,n\} = 2$.

D.2. The Ky Fan norm and its dual

1-balls in l_∞, l_1 and l_2 norms are well-known from textbooks. But what about the Ky Fan k-norm? How can it be represented?

To showcase the complex structure of the Ky Fan k-norm and its dual, we suggest the illustrations Figure 8 with the ball in the Ky Fan 2-norm in Figure 8(a)subfigure and its dual in Figure 8(b)subfigure. On x-, y-, and z-axes, there are singular values σ_1, σ_2, and σ_3 respectively of a matrix from $\mathbb{R}^{m\times n}$ with $\min\{m,n\} = 3$. In this particular case, we do not sort the singular values. In the proposed representation, we actually plot balls in the Top-2 norm $\max\{|x|+|y|, |x|+|z|, |y|+|z|\}$ and its dual norm $\max\{\max(|(|x|), |y|, |z|), \frac{1}{2}(|x|+|y|+|z|)\}$. The resulting balls are much more complex than balls in l_∞, l_1 and l_2 norms.

In fact, those balls can be described easier if we use the results from (Yu, 2012). The Ky Fan 2-norm ball is an intersection of three l_1 balls in (x,y), (x,z), and (y,z) spaces. The 1-ball in the dual Ky Fan 2-norm is an intersection of 1-ball the in l_∞ norm and $\frac{1}{2}$-ball in the l_1 norm.

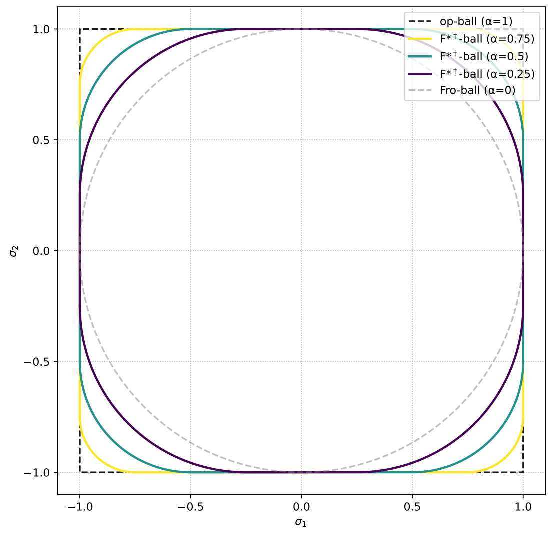

(a) lmo balls for F-Muon for different α

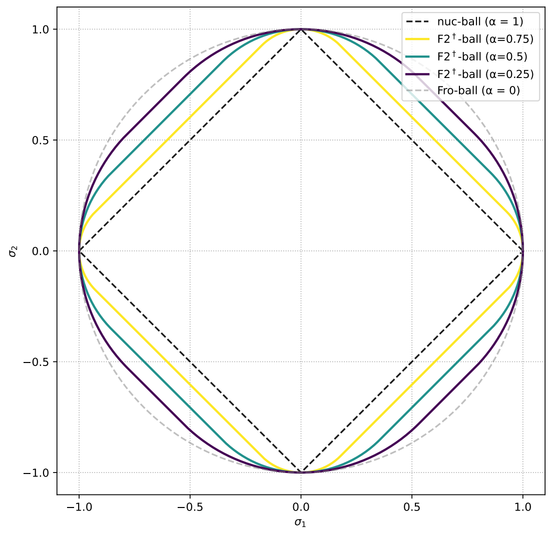

(b) lmo ball for F-Neon for different α

Figure 7: Balls in the duals to F* and F2 norms for different α

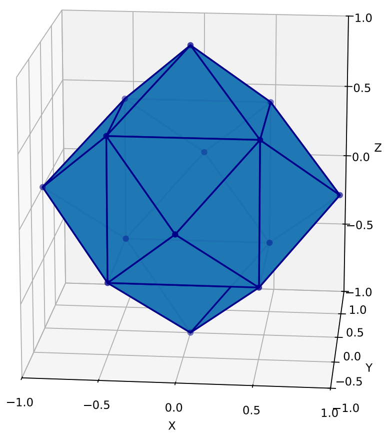

(a) The Ky Fan 2-norm

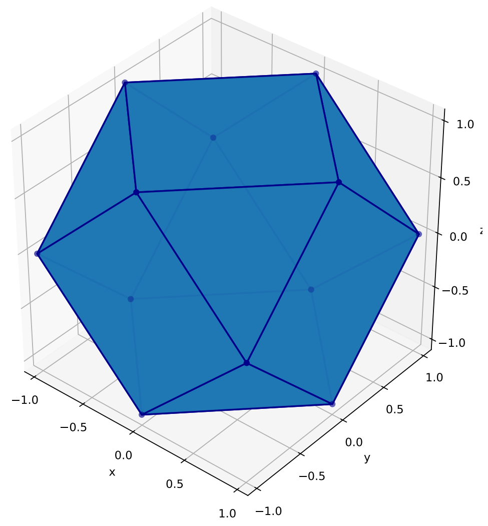

(b) Dual to the Ky Fan 2-norm

Figure 8: Ky Fan 2-norm and its dual

Appendix E. More data for Linear Least Squares

Table 5: Tuning lrs and momentum coefficients

Algorithm	`lr`	`momentum`	Iterations to 0.001 loss
Muon	0.007	0.5	1060
NSGD	0.08	0.95	1020
F-Muon	0.015	0.7	910
SignSGD	0.016×0.01	0.95	2650
S-Muon	0.011	0.9	890

Appendix F. Under the hood of CNN on CIFAR-10

Most bounds for Muon and other LMO-algorithms are given for the norm of the gradient (Kovalev, 2025; Pethick et al., 2025c; Riabinin et al., 2025; Kovalev and Borodich, 2025). Accordingly, it is natural to measure those norms on a real deep learning problem.

Table 6: Parameters for CIFAR-airbench. `sign_lr_mult` for S-Muon is 0.003

Method	`lr`	`momentum`	val_accuracy, %
NSGD	0.5	0.95	91.6 ± 0.52
SignSGD	0.003	0.95	91.54 ± 0.26
Muon	0.24	0.6	94.01 ± 0.10
F-Muon	0.40	0.6	94.01 ± 0.13
S-Muon	0.42	0.63	94.03 ± 0.13
Neon	0.24	0.6	69.8 ± 0.5
F-Neon	0.40	0.6	87.15 ± 0.24
Fanion-5	0.24	0.6	80.69 ± 1.25
F-Fanion-5	0.40	0.6	86.66 ± 0.65

We compare Muon, F-Muon, S-Muon, NSGD, SignSGD, Neon, and F-Neon, Fanion-5, and F-Fanion-5 on CIFAR-airbench. NSGD and SignSGD are not heavily tuned. The hyperparameters of Neon, F-Neon, Fanion-5, and F-Fanion-5 are taken from Muon and F-Muon. The parameters are in the table Table 6. val_accuracy is for the the weighted variant. However, to preserve the algorithms, we do not normalize the weights of the network each iteration.

We log train and validation accuracy, and nuclear, gradient, and spectral norms of the gradients of conv1.weight and conv2.weight for all the layers. The gradient norms decrease only by the order of ten maximum during training, while train accuracy reaches full 100% for Muon, S-Muon, and F-Muon.

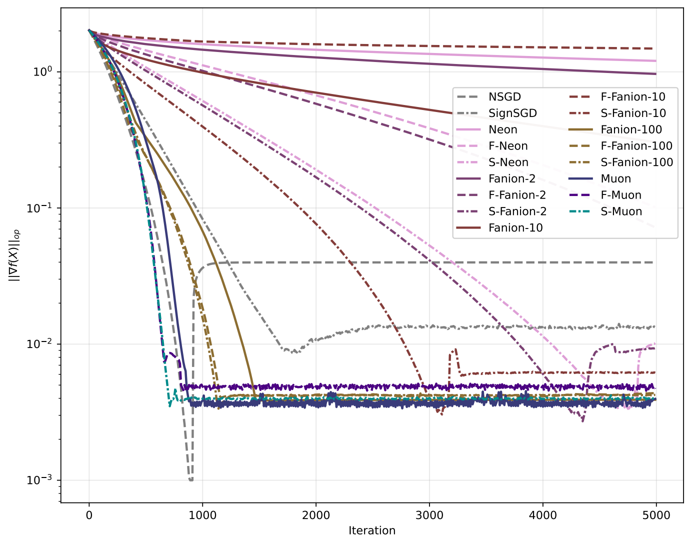

(a) The spectral norm of the gradient

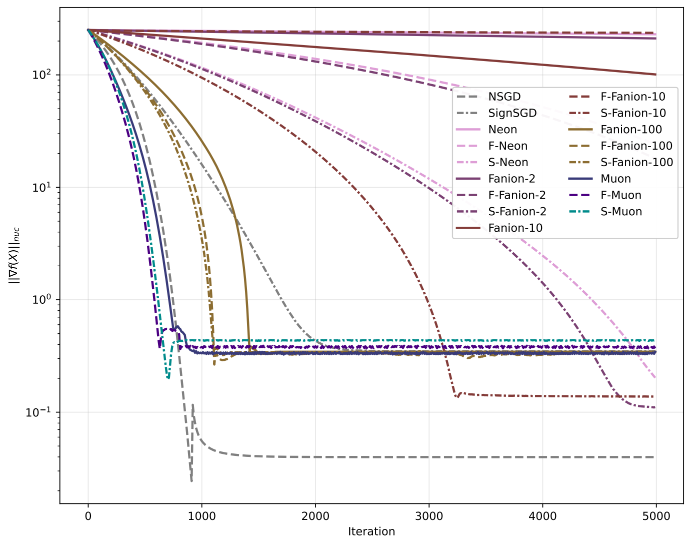

(b) The nuclear norm of the gradient

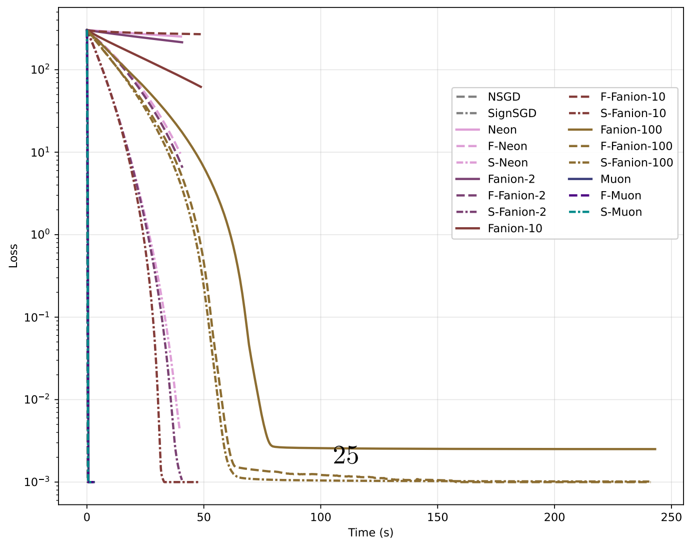

(c) The loss over time

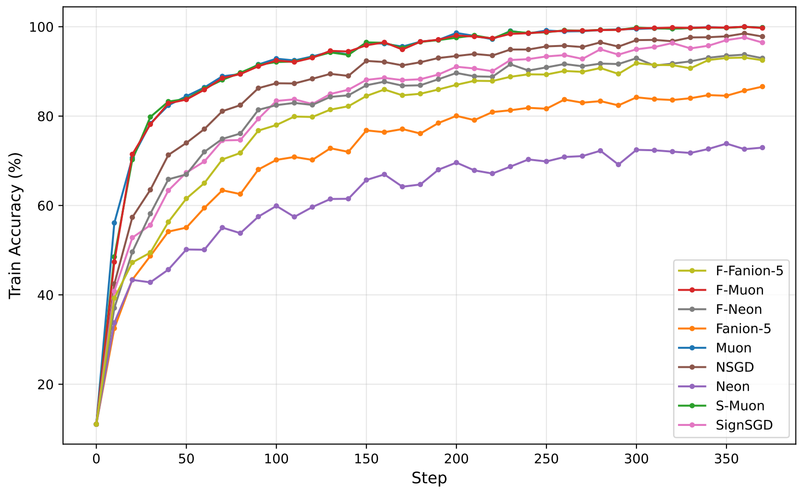

(a) Train accuracy

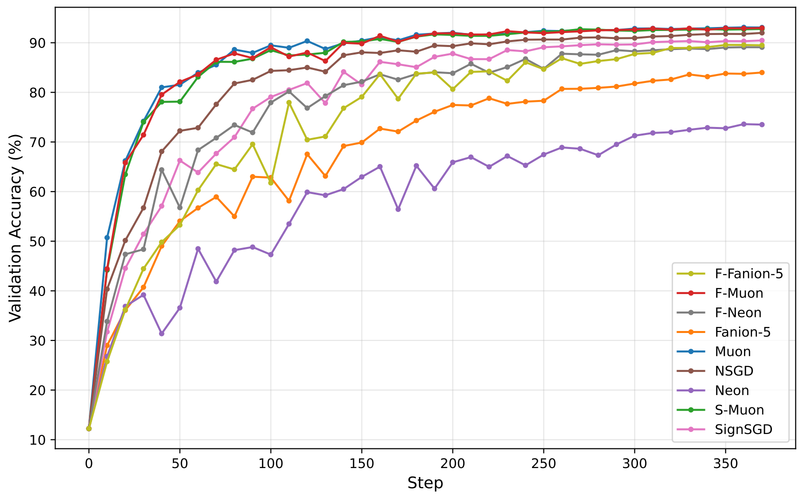

(b) Validation accuracy

Figure 10: Different optimizers on CIFAR airbench without weight normalization

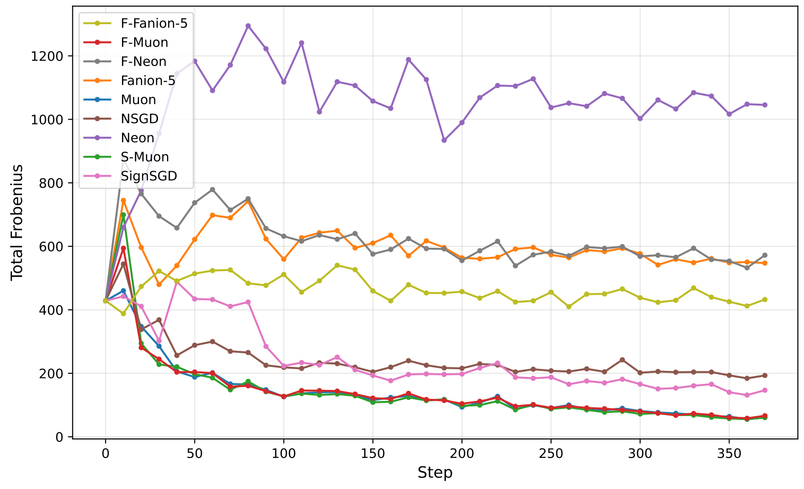

(a) Total Frobenius norm

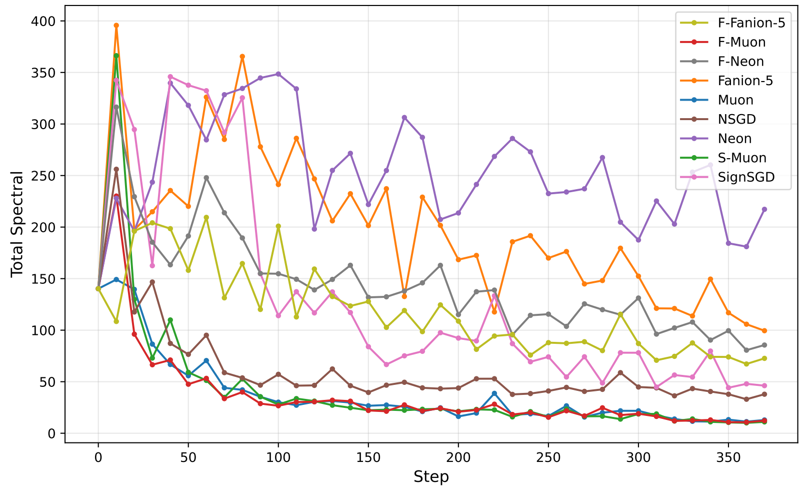

(b) Total spectral norm

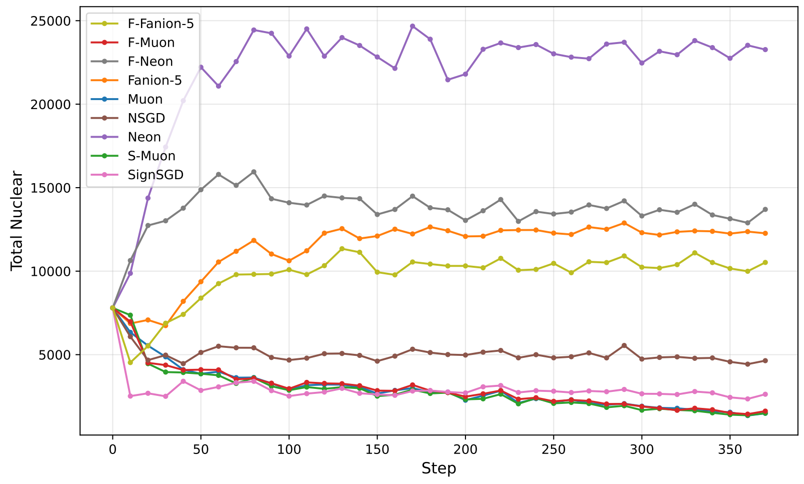

(c) Total nuclear norm

Figure 11: Matrix norms of the whole gradient of CIFAR CNN

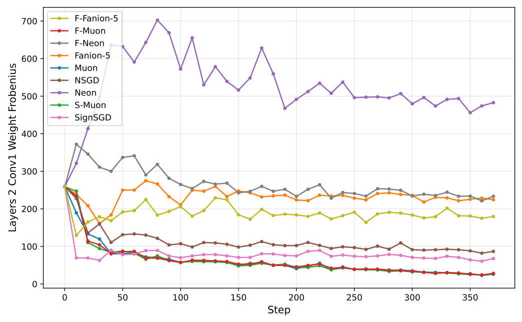

(a) Frobenius norm of layer2.conv1

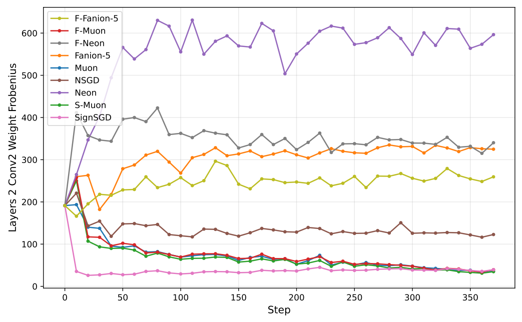

(b) Frobenius norm of layer2.conv2

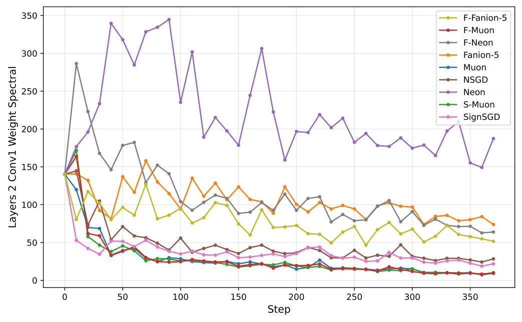

(c) Spectral norm of layer2.conv1

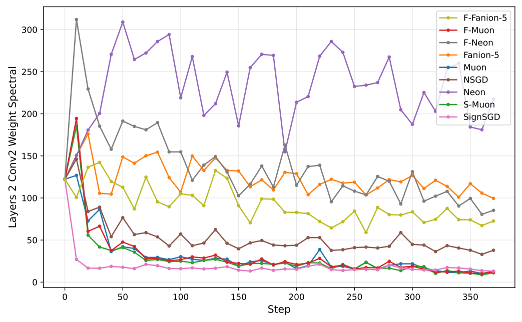

(d) Spectral norm of layer2.conv2

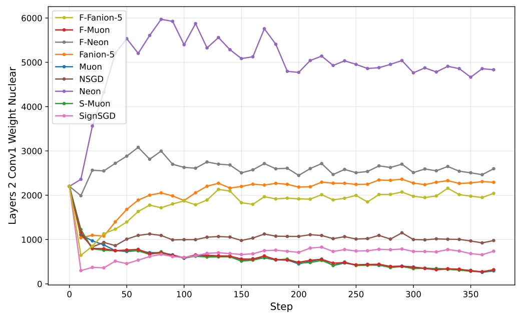

(e) Nuclear norm of layer2.conv1

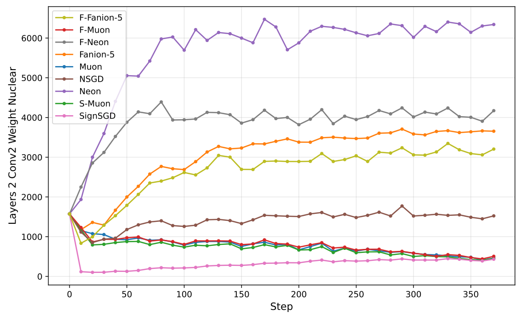

(f) Nuclear norm of layer2.conv2

Figure 12: Matrix norms of layer2.conv1 (left) and layer2.conv2 (right) gradients of CIFAR CNN

Appendix G. Technical details of the experiments

CIFAR airbench We used NVIDIA RTX A4000.

NanoGPT pretrain We used the standard setting of $8 \times$ H100 as documented in (Jordan et al., 2024a).

NanoGPT Fine-tuning. Experiments were conducted on a single NVIDIA RTX 4090 (24GB) GPU using PyTorch 2.8 with CUDA 12.8 and cuDNN 9.0, running on a workstation equipped with an Intel Core i9-14900KS CPU and 128 GB of RAM. No distributed or mixed-hardware training setups were used, ensuring a strictly controlled and unbiased comparison across optimizers.

A uniform training protocol was applied to all runs, including identical batch size, warm-up and cosine decay learning rate schedule, gradient clipping strategy, and validation split. Our optimization methods were integrated into the NanoGPT training loop without modifying the model architecture or preprocessing pipeline. Model quality was primarily evaluated using validation loss tracked over 200 training steps.